Environ Sci Pollut Res (2016) 23:2628–2639
DOI 10.1007/s11356-015-5443-1

RESEARCH ARTICLE

Characteristics of simultaneous ammonium and phosphate adsorption from hydrolysis urine onto natural loess

Shanqing Jiang[1] · **Xiaochang Wang**[1] · **Shengjiong Yang**[1] · **Honglei Shi**[1]

Received: 30 May 2015 / Accepted: 15 September 2015 / Published online: 3 October 2015

Abstract Nutrient recovery from human urine is a promising pretreatment of domestic wastewater and provides a sustainable recyclability of N and P. In this study, batch experiments were conducted to identify the characteristics of natural loess (NL) for the adsorption and recovery of ammonium and phosphate from hydrolysis urine (HU). The adsorption mechanisms, the adsorption kinetics and isotherms, as well as the major influencing factors, such as pH and temperature, were investigated. Results revealed that adsorption of ammonium occurred by means of ion exchange and molecule adsorption with the ≡Si–OH groups, while phosphate adsorption was based on the calcium phosphate precipitation reaction and formation of inner-sphere complexes with≡M–OH groups. The adsorption processes of ammonium and phosphate were well described by the pseudo-second-order kinetic model and the Freundlich isotherm model. Adsorption of phosphate was endothermic, while ammonium adsorption was exothermic. Furthermore, the maximum ammonium and phosphate adsorption capacities of NL was 23.24 mg N g^{-1} and 4.01 mg P g^{-1} at an initial pH of 9 and 10, respectively. Results demonstrated that nutrient-adsorbed NL used as compound fertilizer or conventional fertilizer superaddition was feasible for its high contents of N and P as well as its environmental friendliness.

Keywords Hydrolysis urine · Nitrogen recovery · Phosphorus recovery · Natural loess · Adsorption mechanisms · Fertilizer

Introduction

Human urine is the fraction of domestic wastewater which contains the major part of nutrient with approximately 80 % of nitrogen (N) and 50 % of phosphorus (P) (Dbira et al. 2014). Traditional option of transporting urine to a centralized wastewater treatment plant (WWTP) is economically improvidence and environmental unsustainability, for which increases infrastructure investment and complicates nutrients removal (Udert and Wachter 2012). However, N and P are essential elements for the growth of all living organisms, and P is a nonrenewable resource which may be depleted in 100 years (Deng and Shi 2015; Yang et al. 2013a). Therefore, nutrient recovery from human urine is potential and urgent; not only can it be a promising pretreatment of domestic wastewater, but it also promotes the sustainable recyclability of N and P resources.

In hydrolysis urine (HU), N and P are mainly present in the inorganic forms of ammonium and phosphate, respectively (Maurer et al. 2006). In the last decades, various technologies have been developed for N and P recovery from HU, primarily including dehydration (evaporation (Antonini et al. 2012), freeze thaw (Lind et al. 2001)), magnesium ammonium phosphate (MAP) crystallization (Triger et al. 2012), electrochemical (Kuntke et al. 2014) and combined processes (freezing+MAP (Ganrot et al. 2007), electrochemical+MAP (Hug and Udert 2013), and nitrification+distillation (Udert and Wachter 2012)). However, their application has been impeded in developing nations due to the complicated operation and high cost (Antonini et al. 2012; Maurer et al. 2006). In this case, adsorption is an alternative technique and has been shown to be superior to the mentioned techniques because of its

Responsible editor: Philippe Garrigues

✉ Xiaochang Wang
xcwang@xauat.edu.cn; 13991976150@163.com

[1] Key Lab of Northwest Water Resources, Environment and Ecology, Ministry of Education, Xi'an University of Architecture and Technology, Xi'an 710055, China

flexibility of design and ease of operation (Deng and Shi 2015). The success of an adsorption technology depends on the selection of an appropriate adsorbent. In recent years, diverse materials were tested for ammonium or phosphate recovery from wastewater or HU, including activated carbon (Boopathy et al. 2013; Wang et al. 2012), resin (O'Neal and Boyer 2013), and natural clay minerals (Alshameri et al. 2014; Kamiyango et al. 2009; Perassi and Borgnino 2014; Wang et al. 2014a; Yin and Kong 2014). Among them, clay minerals, such as kaolinite (Kamiyango et al. 2009), montmorillonite (Perassi and Borgnino 2014), zeolite (Alshameri et al. 2014), palygorskite (Wang et al. 2014a), and attapulgite (Yin and Kong 2014), have increasingly received attention because these natural adsorbents could be directly considered as fertilizers in agriculture after nutrient adsorption (Wang et al. 2014a; Zhao et al. 2013), indicating a new application for the used adsorbents.

Natural loess (NL) is one type of clay minerals, and it is economical, environmentally friendly, and plentiful in the northern part of China. NL primarily consists of various metal oxides and possesses functional physical-chemical properties, such as large surface area, excellent osmosis, high porosity, and water retention ability (He et al. 2012; Tang et al. 2009). NL is the medium for the ammonium and phosphate uptake during direct application of HU as liquid fertilizer in agriculture (Akpan-Idiok et al. 2012; Sangare et al. 2014), indicating an excellent adsorption capacity. Park and Jung (2011) have reported that NL was an available adsorbent for phosphate adsorption from domestic wastewater. However, few studies have reported the utilization of NL for ammonium adsorption and the mechanisms of ammonium and phosphate adsorption onto NL were ignored. Additionally, the concentrations of ammonium and phosphate in HU are hundreds of times greater than in domestic wastewater (Maurer et al. 2006). In this study, NL was used as an adsorbent for the simultaneous adsorption and recovery (A/R) of ammonium and phosphate from HU, and the overarching objectives were to determine the capacity of NL for ammonium and phosphate A/R from HU and deeply analyze the mechanisms of the process. The surface characteristics, along with the kinetic, isotherm, and thermodynamic models, were investigated. In addition, the influencing factors (such as pH, contact time, and temperature) and the feasibility of the nutrient-adsorbed natural loess (NANL) as fertilizer were also discussed.

Materials and methods

HU and NL

Undiluted urine was freshly collected before experimentation from a waterless urinal in a public toilet of a campus. HU was obtained by storing the fresh urine in a sealed container for 1 month at room temperature to achieve a stable ammonium concentration. Because there were some precipitates in the HU, membrane filtration (through a 0.45-μm filter) was required to achieve accurate data before the adsorption experiment. Table 1 shows the main physical-chemical characteristics of the stable HU. NL was excavated 20 cm from the ground surface (surface impurities were removed) in the campus and was dried in an oven at 104±1 °C until reaching a constant weight. The dried NL particles were crushed, and particles with sizes less than 75 μm were sieved, which were used directly in the adsorption experiment without any physical or chemical modification.

Adsorption experiments

For each batch adsorption experiment, 1 g of accurately weighed NL was added into a cylindrical plastic bottle containing 50 mL of a prescribed initial concentration of HU at the desired pH. The bottle was closed and manually shaken gently and was then placed statically at the required temperature. Each of the batch adsorption experiments was performed in parallel. Samples were filtered immediately after adsorption using 0.45-μm filters to separate NL from HU. The pH and the ammonium and phosphate levels were measured for all of the treated and control samples. The control samples consisted of HU with no NL; these samples were mixed for the maximum duration of the adsorption experiment.

This study mainly investigated the influence of pH, contact time, and temperature on the ammonium and phosphate A/R onto NL. Because the concentration ratio between ammonium and phosphate in HU was constant at the same dilution ratio, the initial concentrations of ammonium and phosphate were determined by the method of fixed dilution ratio. The initial pH of HU was adjusted over the range from 2.0 to 13.0 using different amounts of 0.5~12 M HCl and 0.5~10 M NaOH, and the test tubes were capped to avoid evaporation. Table 2 listed the detailed experimental conditions for each batch adsorption experiment. In addition, the NL and NANL samples of the optimum pH (raw HU pH) were characterized accordingly.

Table 1 Main physical-chemical characteristics of the stable HU

	Mean	±SD
pH	9.13	
Total Nitrogen (mg L^{-1})	6172.16	230.12
Ammonium (mg L^{-1})	5829.21	210.23
Total Phosphorus (mg L^{-1})	396.03	52.32
Phosphate (mg L^{-1})	381.48	46.14

Table 2 Experimental conditions of ammonium and phosphate adsorption from HU onto NL

Main factor	Experimental conditions				
	Time (min)	Initial concentration	pH	Temperature (K)	Loess dosage (g L^{-1})
Contact time	1–1440	1×[a]	9.13	25	20
Initial concentration	1440	1×, 1.5×, 2×, 3×, 4×, 6×, 10×	9.13	25	20
pH	1440	1×	2–13	25	20
Temperature	1440	1×	9.13	15, 25, 35	20

[a] × is diluted times, 1× indicates the raw HU, and 2× indicates the HU that was diluted by an equal amount of distilled water

HU hydrolysis urine, *NL* natural loess

Adsorption models

Kinetic models

To evaluate the efficiency of the ammonium and phosphate adsorption processes in HU onto NL, the pseudo-first-order model (Eq. 1) (Yang et al. 2013b), the pseudo-second-order model (Eq. 2) (Yang et al. 2013b), and the intra-particle diffusion model (Eq. 3) (Zhao et al. 2013) were used to describe the kinetic data, as follows:

$$\log(q_e - q_t) = \log q_e - k_1 t \tag{1}$$

$$t/q_t = 1/k_2 q_e^{\,2} + t/q_e \tag{2}$$

$$q_t = k_p t^{1/2} + c \tag{3}$$

where k_1 is the pseudo-first-order rate constant (min^{-1}), k_2 is the pseudo-second-order rate constant (g min^{-1} mg^{-1}), k_p is the diffusion coefficient of the intra-particle diffusion model (mg $min^{-1/2}$ g^{-1}), t is the contact time (min), and c is the intercept. The parameter q_t is the adsorption amount of ammonium or phosphate at time t (mg g^{-1}) and q_e is the adsorption amount at equilibrium (mg g^{-1}). The value of q_t was calculated according to the following equation (Eq. 4):

$$q_t = (C_0 - C_t)\mathrm{V}/\mathrm{w} \tag{4}$$

where C_0 and C_t are the concentrations of either ammonium or phosphate at the initial time and at certain time t (mg L^{-1}), respectively, V is the volume of HU (mL), and w is the mass of NL (g).

Isotherm models

Adsorption isotherm models can be used to reveal the mechanism of adsorption of ammonium and phosphate in HU onto NL. The Langmuir isotherm (Eq. 5) and Freundlich isotherm (Eq. 6) (Zhao et al. 2013) models were chosen to describe the adsorption equilibrium data, as follows:

$$1/q_e = 1/q_{max} + 1/(K_L q_{max} C_e) \tag{5}$$

$$q_e = K_F \cdot C_e^{\,1/n} \tag{6}$$

where q_e is the adsorption amount of ammonium or phosphate on the NL at equilibrium (mg g^{-1}), q_{max} is the maximum adsorption capacity (mg g^{-1}), and C_e is the concentration of ammonium or phosphate in HU at equilibrium (mg L^{-1}). K_L is the Langmuir constant related to the adsorption energy (L mg^{-1}), K_F ($mg^{1-1/n}$ $L^{1/n}$ g^{-1}) is the Freundlich adsorption isotherm constant indicating the adsorption capacity of the adsorbents and which is always related to the temperature and the physical-chemical characteristics of adsorbents, and the parameter n is the Freundlich exponent related to the intensity of adsorption (Huang et al. 2014). The value of q_e was calculated using Eq. 4 with C_t replaced by C_e.

Thermodynamic models

To further confirm the feasibility of the adsorption process, the thermodynamic parameters of adsorption of ammonium and phosphate in the HU onto NL were calculated by the following equations (Eqs. 7–10) (Huang et al. 2014):

$$K_e = q_e/C_e \tag{7}$$

$$\Delta G^o = -\mathrm{R}T\ln K_0 \tag{8}$$

$$\Delta G^o = \Delta H^o - T\Delta S^o \tag{9}$$

$$\ln K_0 = -\Delta H^o/\mathrm{R}T + \Delta S^o/\mathrm{R} \tag{10}$$

where K_e is the equilibrium constant (dimensionless), ΔG^o is the change in Gibb's free energy (kJ mol^{-1}), R is the universal gas constant (8.314 J mol^{-1} K^{-1}), and T is the temperature of the experiment (K). ΔH^o is the change in enthalpy (kJ mol^{-1}) and ΔS^o is the change in entropy (kJ mol^{-1} K^{-1}), and the

values of ΔH^o and ΔS^o were calculated from the slope and intercept of $\ln K_0$ against $1/T$.

Analytical methods

X-ray diffraction (XRD; Empyrean, PANalytical B.V., Holland) was used to study the mineralogical composition of the NL. Scanning electron microscope (SEM; Quanta 600 FEG, FEI, USA) observations and semiquantitative energy-dispersive X-ray spectrometry (EDX; INCA Energy 350, Oxford, UK) electron microprobe analyses were performed on NL samples to evaluate the microcosmic morphological changes during adsorption. The specific surface area of the NL before and after adsorption was determined using a Brunauer–Emmett–Teller (BET) specific surface analysis device (V-Sorb 2800P, GAPP, China) using the He-N_2 method. In addition, the elemental species changes of NL and NANL were analyzed by X-ray photoelectron spectroscopy (XPS; K-Alpha, Thermo Scientific, USA), and the XPS spectra peaks of N 1 s, P 2p, O 1 s and Ca 2p were further divided using the XPSpeak software. The concentrations of ammonium and phosphate were detected with Nessler's reagent and ascorbic acid spectrophotometry, respectively (TU-1901, Persee, China) (MEPC and WWMAA 2002). All of the tests were performed in triplicate, and the data are expressed as the mean of observed values and followed by the standard deviation (±SD).

Results and discussion

Characterization of NL and NANL

The XRD spectrum of the NL is shown in Fig. 1a. It indicated that the main mineral species in the NL were albite, aluminum oxide, calcite, illite, kaolinite, and quartz, which were similar to the results of He et al. (2012) and Tang et al. (2009). The surface morphology of the NL and NANL was examined by SEM (Figs. 1b, d); it was observed that the heterogeneous and irregularly sized surfaces of the NL were covered with a rough texture (Fig. 1b), while many fine spherical clusters were distributed on the surface of the NANL in Fig. 1d. In addition, the EDX analysis, shown in Fig. 1c, revealed that metal oxides are the major composition of NL, and the atomic percent of Si, Ca, Al, and Fe was 33.92, 4.15, 4.97, and 1.81 %, respectively. In contrast to Fig. 1c, the EDX analysis in Fig. 1e demonstrated that the spherical clusters on the surface of NANL are primarily composed of O, Ca, and P, with the exception of Si, indicating a possible calcium phosphate precipitation formation (Yin and Kong 2014), and the detail reaction processes will be analyzed in the following section. Furthermore, the specific surface area of the NL and NANL was also detected and is shown in Table 3, revealing that the BET decreased from 29.97 to 22.32 $m^2\ g^{-1}$ and the total pore volume decreased from 0.098 to 0.076 mL g^{-1} after the A/R of ammonium and phosphate. These results indicated an effective adsorption process, which was in agreement with the SEM observation in Fig. 1d.

Effect of pH and A/R mechanisms

Generally, the adsorption amount of different compounds (ammonium and phosphate) from aqueous solution is highly dependent on the pH of the solution, which affects the surface charge of the adsorbent as well as the degree of ionization and speciation of the adsorbate (Uğurlu and Karaoğlu 2011). The pH_{zpc} of the NL was 3.12, implying that the surface of the NL particle had a positive charge in HU with a pH≤3.0 and that it was negatively charged in HU with a pH≥4.0 (Alshameri et al. 2014). The phosphate dissociation equilibrium in different pH solutions can be represented by Eqs. 11–13. The $H_2PO_4^-$ and HPO_4^{2-} species are the main species over the pH range from 5 to 10. In detail, the concentrations of $H_2PO_4^-$ species prevail at pH values between 5 and 7, while the HPO_4^{2-} species are dominant at pH values between 7 and 10. For pH values ranging from 10 to 12, the HPO_4^{2-} species prevail over PO_4^{3-}, and the PO_4^{3-}species become significant when the pH is higher than 12 (Yang et al. 2013b). On the other hand, the dominant form of ammonium is NH_4^+ at pH< 9.0, while NH_3 is prevalent at pH>9.0 (Lin et al. 2013).

$$H_2PO_4^- + H_2O \leftrightarrow H_3PO_4 + OH^- \quad pK_1 = 2.16\ (pH \leq 5) \tag{11}$$

$$HPO_4^{2-} + H_2O \leftrightarrow H_2PO_4^- + OH^- \quad pK_2 = 7.20\ (5 < pH \leq 10) \tag{12}$$

$$PO_4^{3-} + H_2O \leftrightarrow HPO_4^{2-} + OH^- \quad pK_3 = 10.3\ \ (pH > 10) \tag{13}$$

For phosphate A/R, the maximal A/R capacity occurred at pH 10.0, which achieved 4.01 mg P g^{-1} for 381.48 mg P L^{-1} of the initial concentrations in HU, and the A/R capacity of phosphate decreased with a further increase or decrease of the initial HU pH (when the pH>11.0 or pH<9.0) (Fig. 2).

1. When the HU pH was lower than pH_{zpc}, the NL surface had a positive charge (hydroxyl protonation (Eq. 14) (Huang 2004)). Most of the $H_2PO_4^-$ species had converted to H_3PO_4 which was a noncharged form, and a portion of $H_2PO_4^-$ was adsorbed onto NL via electrostatic attractions (Eq. 15), while ion exchange was not favored under these conditions

$$\equiv M - OH\ +\ H^+ \rightarrow \equiv M - OH_2^+ \tag{14}$$

$$\equiv M\text{–}OH_2^+ \bullet\bullet\bullet H_2PO_4^- \tag{15}$$

where M is a metal component, such as Ca, Al, or Fe.

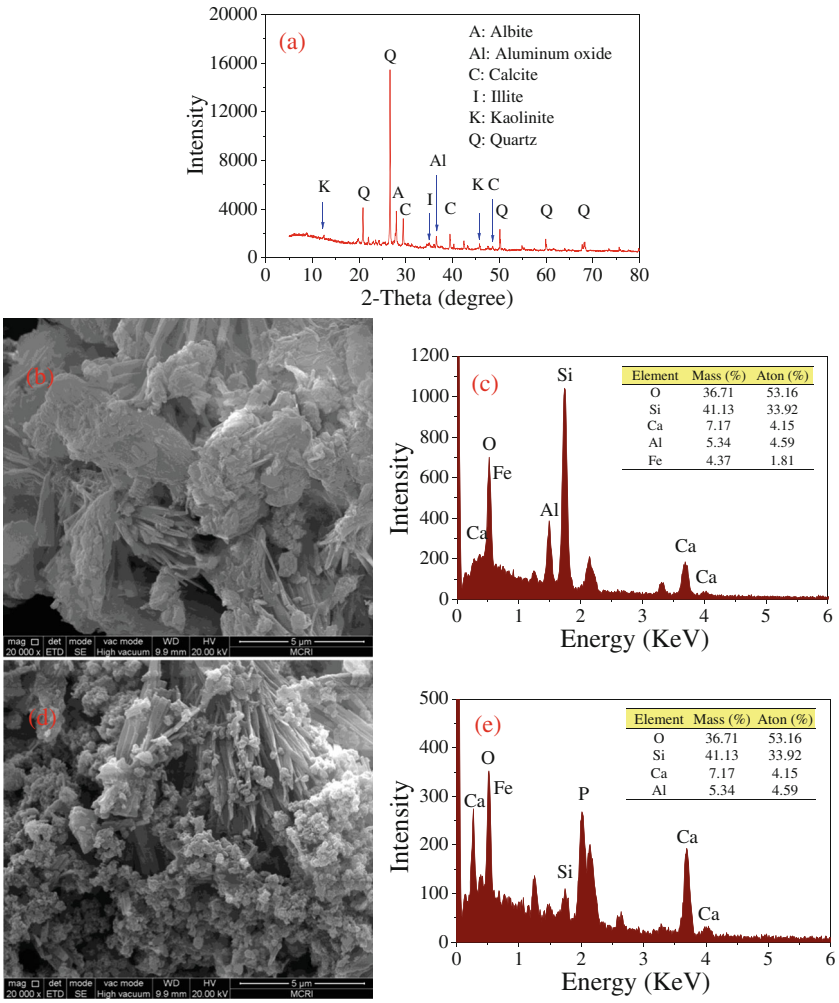

Fig. 1 NL characterization: **a** XRD results of NL; **b** SEM image of NL, 20,000×; **c** EDS analysis of NL; **d** SEM image of NANL, 20,000× (pH=9.13); **e** EDS analysis of NANL (pH=9.13)

2. At pH>pH_{zpc}, the NL surface had a negative charge (hydroxyl deprotonation (Eq. 16) (Huang 2004)). The negative charge of the NL surface was stronger with the increasing HU pH, which would result in an electrostatic repulsion. However, the increased phosphate A/R capacity onto NL at a higher initial HU pH in Fig. 2 suggested that neither ion exchange nor electrostatic attraction controlled phosphate adsorption under these conditions (Lin et al. 2014). The metal oxides in the hydrolysis reaction (Eq. 17) could supply $M^{(2y/x)+}$ and OH^-, which could be used in the inner-sphere ligand exchange reaction. Portions of the ≡M–OH groups on the NL were possibly involved in the formation of inner-sphere species via monodentate (Eq. 18) and bidentate (Eqs. 19 and 20) complexation for phosphate adsorption (Guaya et al. 2015; Lǔ et al. 2013), appearing to be an alternative explanation in this case. On the other hand, according to the SEM and EDX analysis results of NANL (Fig. 1d, e), Ca^{2+}, OH^-, and HPO_4^{2-} might react chemically under alkaline conditions, forming hydroxyapatite ($Ca_{10}(OH)_2(PO_4)_6$, HAP) (Eq. 21), which has the highest thermodynamic stability among various calcium phosphate precipitations (Barca et al. 2012). Additionally, reaction (Eq. 21) can occur at pH>7.0 which is also favorable only at pH>9.0 (Vanotti et al. 2003), which might be the explanation of the result that the A/R capacity of phosphate increased as the pH increases and achieved its maximum at pH 10.0 (pH<10.0) (Fig. 2):

$$\equiv M - OH \rightarrow \equiv M - O^- + H^+ \quad (16)$$

$$M_xO_y + yH_2O \rightarrow xM^{-\left(2y/x\right)} + 2yOH^+ \quad (17)$$

$$\equiv M - OH + H_2PO_4^- \rightarrow \equiv M - O - \underset{\underset{O}{\|}}{\overset{\overset{O}{|}}{P}} - OH + OH^- \quad (18)$$

$$\equiv M-OH + HPO_4^{2-} \rightarrow \equiv M<\begin{matrix}O\\O\end{matrix}>P\leq \begin{matrix}OH\\O\end{matrix} + OH^- \quad (19)$$

$$2\equiv M-OH + HPO_4^{2-} \rightarrow \begin{matrix}\equiv M-O\\\equiv M-O\end{matrix}>P\leq \begin{matrix}OH\\O\end{matrix} + 2OH^- \quad (20)$$

where M is a metal component, such as Ca, Al, or Fe.

$$10Ca^{2+} + 6HPO_4{}^{2-} + 8OH^- \rightarrow Ca_{10}(OH)_2(PO_4)_6\downarrow + 6H_2O \quad (21)$$

3. The decrease of phosphate A/R capacity with the increase of HU pH above 11.0 (Fig. 2) was related to the increasing negative charge of the NL surface, which resulted in an electrostatic repulsion between the NL particle surface and the phosphate ions. In addition, a partial dissolution of the NANL occurred at a pH above 11.0, which caused the decrease of adsorption sites and the release of adsorbed phosphate (Yang et al. 2013b). Furthermore, the competitive adsorption between a high concentration of OH^- and phosphate ions was unfavorable for phosphate A/R onto NL.

For ammonium A/R, the maximum A/R amounts occurred at pH 9.0, with approximately 23.24 mg N g^{-1} for 5829.21 mg N L^{-1} of initial concentrations in HU, and the A/R capacity of ammonium on the NL decreased with a further increase or decrease in the initial HU pH (when pH>10.0 or pH<8.0) (Fig. 2).

1. When pH<pH_{zpc}, the NL surface had a positive charge, and the repulsive forces between the NL particle surface and the NH_4^+ ions depressed the ammonium adsorption capacity.
2. When the pH was higher than pH_{zpc}, ammonium would be adsorbed via electrostatic attraction on the negatively charged NL surface. The zeta potential decreased with the increase of pH, and the number of negative charges on the NL surface increased at a high pH. Therefore, the electrostatic attraction between the NH_4^+ ions and the NL surface was stronger at a higher pH, which results in a higher ammonium A/R capacity (Yang et al. 2015). In addition,

Table 3 BET surface area and total pore volume of the NL before and after ammonium and phosphate adsorption from HU

	BET surface area			Total pore volume (mL g^{-1})
	Values (m^2 g^{-1})	Monolayer volume (mL g^{-1})	R^2	
Before adsorption	29.9697	5.1410	0.9992	0.0984
After adsorption	22.3236	3.8924	0.9995	0.0765

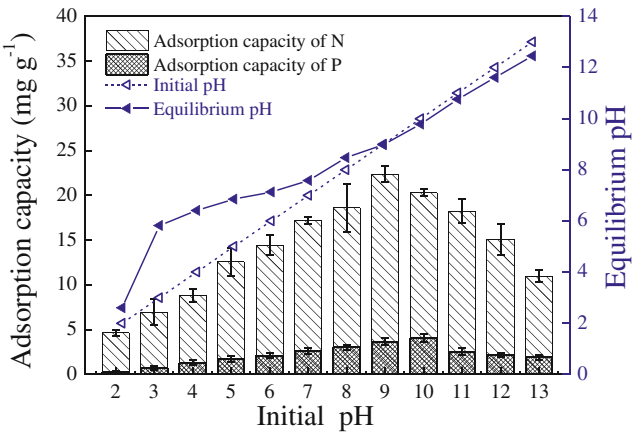

Fig. 2 Effect of pH on ammonium and phosphate adsorption from HU onto NL

with an increase in pH, only a negligible amount of H^+ ions compete with NH_4^+ ions, which facilitate ammonium A/R. Briefly, electrostatic attraction occurs on the NL surface, and ion exchange occurs inside of the NL particles, which can be expressed by the following reaction (Eq. 22) (Lin et al. 2013):

$$NL-M^{n+} + nNH_4{}^+ \rightarrow NL-nNH_4{}^+ + M^{n+} \quad (22)$$

where M is a metal component, such as Ca, Al, or Fe. Moreover, the ion exchange between Ca^{2+} and NH_4^+ would further promote the precipitation reaction of phosphate (Eq. 21) (Lin et al. 2014); thus, the presence of ammonium also has a positive influence on the A/R of phosphate.

3. The ammonium A/R capacity decreased with a further increase in HU pH when pH>10.0 (Fig. 2), causing NH_3 to be the predominant species and causing the low ion exchange capability between metal ions and NH_4^+. In addition, the partial dissolution of the NANL occurred, which resulted in the release of ammonium (Huang et al. 2010). However, it can also be found from Fig. 2 that the adsorption capacity remained over 50 % of its maximum at pH 13.0, which indicated that a molecular force (van der Waals' force) was functionalized between ammonia and the NL surface in which some ≡Si–OH groups were utilized as neutral adsorption sites (pH>10.0) (Eq. 23) (Yang et al. 2015).

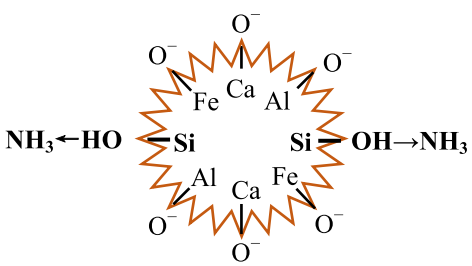

(23)

On the other hand, Fig. 2 also illustrated the relationship between the initial and equilibrium HU pH values for the adsorption of ammonium and phosphate onto NL. Initially, the equilibrium pH value was generally higher than that of the initial pH when the initial pH ranged from 3.0 to 6.0, which was mainly due to the complexation reaction of ≡M–OH groups and phosphate ions on the NL surface (Eqs. 18–20), further confirming that the inner-sphere ligand exchange was occurred here. In addition, the equilibrium pH value was slightly higher than that of the initial pH from 7.0 to 10.0, complexation reaction (Eqs. 18–20) and chemical precipitation (Eq. 21) were occurred simultaneously, and part of OH^- was consumed by the precipitation reaction. Finally, the equilibrium pH value was less than the initial pH when the pH> 11.0, which could be explained through the following aspects: (1) the released H^+ from the deprotonation of hydroxides (Eq. 16) under higher pH conditions would consume the OH^- of HU; and (2) the amounts of molecular NH_3 in the HU was adsorbed (Huang et al. 2010).

Overall, the primary mechanisms of phosphate A/R on the NL included inner-sphere ligand exchange and chemical precipitation reaction; ion exchange and molecule adsorption probably operated together for the A/R of ammonium. In addition, the ion exchange between Ca^{2+} and NH_4^+ would promote the A/R of phosphate on the NL. Furthermore, the optimum pH of ammonium and phosphate adsorption was close to the raw HU pH; thus, HU could be directly used in the following study and in practice without any pH adjustment.

XPS analysis

For further confirming the A/R mechanisms of ammonium and phosphate discussed in the above section, the XPS spectra (whole scanning, N 1 s, P 2p, Ca 2p, and O 1 s) of the NL before and after adsorption from raw HU (pH=9.13) were analyzed and are illustrated in Fig. 3. Figure 3a shows whole scanning spectra of the NL and NANL; the N 1 s and P 2p peaks obviously appeared in the spectra of the NANL compared with the NL, indicating the presence of N and P on the surface of the NANL. The high precision spectrum of N 1 s of the NANL surface could be divided into two peaks (399.5 and 400.7 eV), which corresponded to NH_3 and NH_4^+, respectively (Fig. 3b) (NIST 2012). This result indicated that ionic NH_4^+ and molecular NH_3 were adsorbed on the NL, and ion exchange and molecule adsorption probably operated together for ammonium adsorption. Figure 3c, d shows the high precision spectra of P 2p and Ca 2p of the NANL surface, respectively. The P 2p spectrum of the NANL surface could be divided into two peaks (132.9 and 133.8 eV) which corresponded to PO_4^{3-} and HPO_4^{2-}, respectively (Hanawa and Ota 1991; Xie et al. 2013; Yin and Kong 2014), and a new peak of 347.2 eV appeared in the Ca 2p spectrum of NANL compared with the Ca 2p spectrum of NL. In addition, the Ca 2p peak of 347.2 eV and the P 2p peak of 132.9 eV almost agreed with the values for HAP (Ohtsu et al. 2012), implying that HAP precipitation was formed and chemical precipitation reaction was presented in phosphate A/R. Further, based on the blinding energy of different oxygen species, the O 1 s XPS spectra were further divided into three peaks (530.1, 531.7, and 533.2 eV), which corresponded to M─O (oxygen bonded to metal), M─OH (hydroxyl bonded to metal), and H_2O, respectively (Lǔ et al. 2013; Su et al. 2013) (Fig. 3e). For the NL, the percentages of M─O, M─OH, and H_2O were separately 14.7, 74.9, and 10.4 %, respectively; however, the percentages of M─O, M─OH, and H_2O after nutrient adsorption changed to 24.9, 63.3, and 11.8 %, respectively. This result suggested that M─OH groups existed on the surface of NL and the M─OH percentage dropped sharply by the adsorption of phosphate, which further demonstrated that the M─OH on the NL surface participated in the phosphate adsorption and accordingly caused the replacement of hydroxyl groups by phosphate ions, revealing that the monodentate or bidentate complexes between phosphate and the M─OH groups on the NL surface might be formed (Lǔ et al. 2013; Su et al. 2013). Thus, the XPS analysis further supported the results in the previous section.

Effect of contact time and adsorption kinetics

The adsorption capacity of ammonium and phosphate on NL was investigated as a function of contact time under the conditions given in Table 2 (Fig. 4a). It was found that the adsorption process for NL could be divided into two steps in which the adsorption increased rapidly during the first 60 min then changed gradually until the plateau of adsorption equilibrium was attained. This observation was in well agreement with the previous report by Wang et al. (2014a) and Lǔ et al. (2013). The fast adsorption rate during the first step could be attributed to the presence of more available vacant active sites on the NL surface, and surface adsorption plays the main role for the ammonium and phosphate uptake; however, a decrease in unsaturated adsorption sites on the surface of NL occurred in the second step.

The kinetics data of ammonium and phosphate adsorption onto NL were further modeled using the pseudo-first-order model (Eq. 1) and the pseudo-second-order model (Eq. 2) (Fig. 4a). The corresponding parameters and correlation coefficients (R^2) are listed in Table 4. As shown in Table 4, the values of R^2 for the pseudo-second-order model were higher than 0.999 and the calculated ammonium and phosphate equilibrium adsorption capacity of the pseudo-second-order model was 23.33 mg N g^{-1} and 3.90 mg P g^{-1}, respectively, which were close to the experimental values of 23.24 mg N g^{-1} and

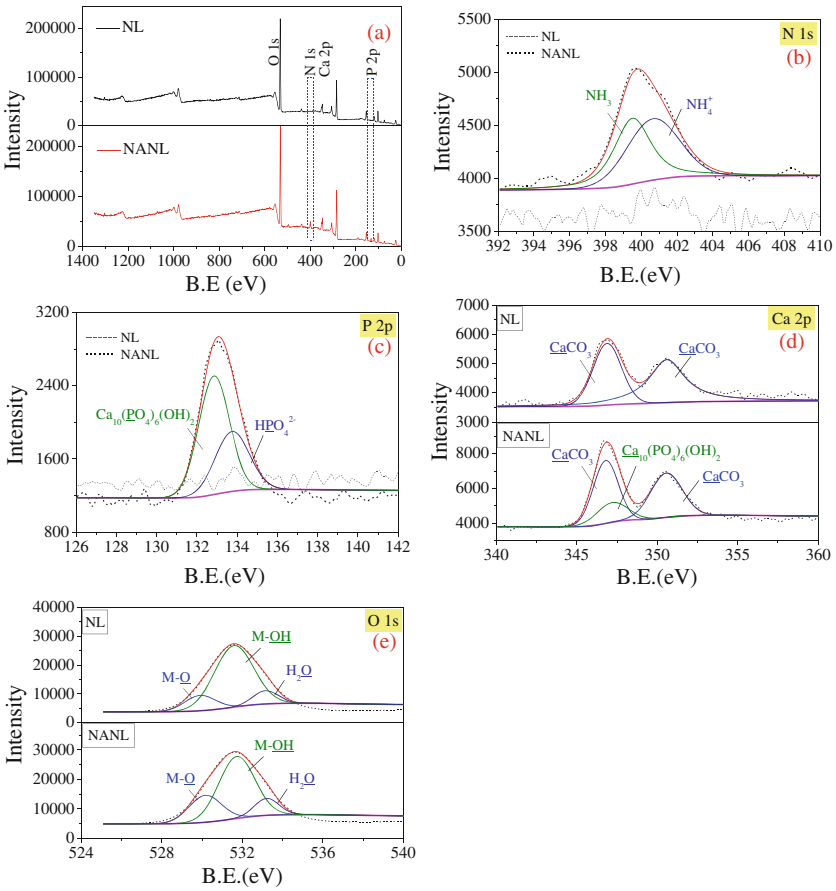

Fig. 3 XPS spectra of NL before and after the adsorption of ammonium and phosphate in raw HU (pH=9.13): **a** whole scanning, **b** the N 1 s, **c** P 2p, **d** Ca 2p, and **e** O 1 s spectra analysis of NL and NANL

4.01 mg P g^{-1}, respectively. The results indicated that ammonium and phosphate adsorption onto NL were well described by the pseudo-second-order model. Similar kinetic study results have been reported by Guaya et al. (2015). Therefore, chemisorption could be the dominant mechanism in addition to physical adsorption (Wang et al. 2014a), which was in accord with the analysis in "Effect of pH and A/R mechanisms".

To further understand the adsorption process of ammonium and phosphate onto NL, the intra-particle diffusion model (Eq. 3) was also employed to fit the experimental data in Fig. 4b. As shown in Fig. 4b, the linear fit of the intra-particle diffusion model for ammonium and phosphate adsorption showed two linear portions, indicating their multi-stage adsorption processes, consistent with the results in Fig. 4a. The first stage was attributed to the diffusion of ammonium and phosphate from the HU external or boundary layer to the external surface of the NL, and the second stage was ascribed to the intra-particle diffusion effects and gradual attainment of the equilibrium stage. Similar explanations were reported in other studies (Liu et al. 2013; Wang et al. 2014a). Further, seen from Fig. 4b and Table 4, the fitting lines did not pass through the origin, and the constants of C were not zero, indicating that the intra-particle diffusion was not the rate-limiting step for ammonium and phosphate adsorption, and the adsorption process may consist both surface adsorption and intra-particle diffusion (Liu et al. 2013).

Adsorption isotherms

To provide a better understanding of ammonium and phosphate adsorption onto NL, the Langmuir and Freundlich isotherm plots are given in Fig. 4c, d, and the calculated parameters of these models are presented in Table 4. The Freundlich model fitted the ammonium and phosphate adsorption data (R_{NF}^2=0.9919, R_{PF}^2=0.9826) better than the Langmuir model did (R_{NL}^2=0.9198, R_{PL}^2=0.9180) (Table 4). This result indicated that ammonium and phosphate adsorption from HU onto NL might not occur in a homogeneous monolayer, but might rather occur in a heterogeneous complex manner (Boopathy et al. 2013; Wang et al. 2012). The heterogeneous surface of NL (Fig. 1b) might possess different types of adsorption sites, and two or more adsorption sites might simultaneously affect the ammonium (ion exchange and molecule adsorption) and phosphate (complexation reaction and chemical precipitation) adsorption. Similar studies (Uğurlu and Karaoğlu 2011; Yang et al. 2013a) also reported that the Freundlich model had a much better fit than the Langmuir model had regarding ammonium and phosphate adsorption.

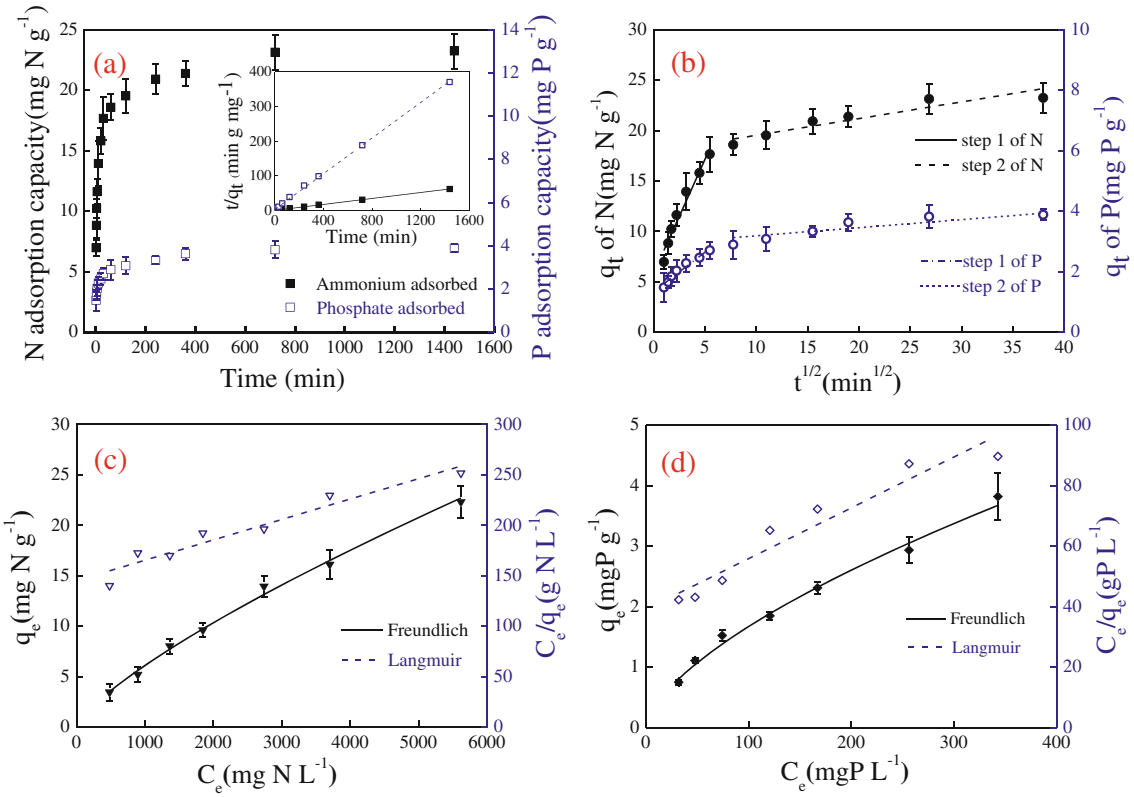

Fig. 4 The results of ammonium and phosphate adsorption from HU onto NL: **a** the effect of contact time and calculation of the pseudo-second-order kinetic model; **b** calculation of the intra-particle diffusion model; **c** calculation of the Langmuir and Freundlich isotherm models of ammonium; **d** calculation of the Langmuir and Freundlich isotherm models of phosphate (*symbols* are experimental data, and *lines* are model results)

In addition, the favorability of the reaction was also important for the adsorption process. For the Freundlich model, the 1/n constant was the indicator of the adsorption intensity, and a value of 1/n between $0.1<1/n<1$ indicated favorable adsorption (Wang et al. 2014a). In this study, the values of 1/n for ammonium and phosphate adsorption were 0.76 and 0.63, respectively, demonstrating that ammonium and phosphate adsorption onto NL was favorable. Therefore, NL demonstrated its potential as an adsorbent for ammonium and phosphate adsorption from HU.

Thermodynamics and effect of temperature

The thermodynamic parameters of ΔG^{o}, ΔH^{o}, and ΔS^{o} were determined using Eqs. 7–10; the results are summarized in Table 4. As shown in Table 4, the values of ΔG^{o} were negative, revealing the favorable and spontaneous process of ammonium and phosphate adsorption onto NL. In detail, the value of $\Delta G_N{}^{o}$ increased from –3.84 to –3.06 kJ mol L^{-1}, and $\Delta G_P{}^{o}$ decreased from –5.57 to –6.91 kJ mol L^{-} as the temperature changed from 288.15 to 308.15 K, indicating the decreasing spontaneity for ammonium but increasing spontaneity for phosphate at higher temperatures. Additionally, the negative value of $\Delta H_N{}^{o}$ and the positive value of $\Delta H_P{}^{o}$ strongly confirmed the exothermic and endothermic nature of ammonium and phosphate adsorption onto NL, respectively. This result was in accordance with the decrease in adsorption capacity for ammonium and the increase for phosphate at higher temperatures (Fig. 5), possibly because the NH_4^+ ion exchange was exothermic and the inner-sphere ligand exchange between ≡M─OH groups and phosphate as well as the HAP precipitation reactions were endothermic. Therefore, room temperature was optimal for ammonium and phosphate adsorption onto NL. Furthermore, the values of ΔS^{o} of ammonium and phosphate were negative and positive, respectively, indicating that the degree of randomness increases at the NL-HU interface during the phosphate adsorption process and that the opposite trend occurs with ammonium. These results were consistent with the adsorption of phosphate from municipal wastewater onto loess (Park and Jung 2011) and the ammonium adsorption process by fly ash and sepiolite (Uğurlu and Karaoğlu 2011).

Evaluation of the NANL as fertilizer

A comparison of the adsorption capacity of the NL with other conventional adsorbents for ammonium and/or phosphate adsorption from HU was presented in

Table 4 Parameters of three kinetics and two isotherms and the thermodynamic models of the adsorption of ammonium and phosphate from HU onto NL

	Pseudo-first-order model			Pseudo-second-order model		
	q_e (mg g^{-1})	k_1 (min^{-1})	R^2	q_e (mg g^{-1})	k_2 (g mg^{-1} min^{-1})	R^2
Ammonium	9.7107	0.0019	0.9085	23.3318	0.0861	0.9993
Phosphate	1.6889	0.0015	0.9199	3.8964	0.0183	0.9990
	Intra-particle diffusion model					
	Step 1			Step 2		
	k_{p1} (mg $min^{-1/2}$ g^{-1})	c_1	R^2	k_{p2} (mg $min^{-1/2}$ g^{-1})	c_2	R^2
Ammonium	2.2617	5.8557	0.9553	0.1577	18.0365	0.8450
Phosphate	0.2596	1.3463	0.9485	0.0334	2.7846	0.8120
	Langmuir isotherm model			Freundlich isotherm model		
	q_{max} (mg g^{-1})	K_L (L mg^{-1})	R^2	K_F (mg g^{-1})	1/n	R^2
Ammonium	49.3827	0.00014	0.9198	0.0316	0.7619	0.9919
Phosphate	5.9523	0.0043	0.9180	0.0882	0.6390	0.9826
	ΔG^o (kJ mol L^{-1})			ΔS^o (K J mol^{-1})	ΔH^o (kJ mol^{-1})	
	288.15 K	298.15 K	308.15 K			
Ammonium	−3.84	−3.45	−3.06	−39.02	−15.08	
Phosphate	−5.57	−6.24	−6.91	66.71	13.64	

Table 5. As the results showed, the adsorption capacity for both ammonium and phosphate of the NL in the present study was apparently more effective than that of natural zeolite and activated carbon (Tettenborn et al. 2007). For selective adsorption onto ammonium or phosphate, clinoptilolite (Beler Baykal et al. 2009) and HAIX-Fe resin (O'Neal and Boyer 2013) exhibited a slight sufficient adsorption capacity than that of NL, respectively. However, the performance of NL for simultaneous N and P recovery was an important advantage than those adsorbents mentioned above. Furthermore, when it comes to the cost, NL is abundant and naturally available in the northern part of China; thus, the cost of NL is acceptable in comparison to resin, active carbon, and other adsorbents. On the other hand, the main species of N and P in NANL were ammonium salts, metal complex of phosphate, and HAP, which were easily absorbed by plants. In total, the NANL could be taken into account as fertilizer for agricultural purposes. For further evaluation of the application potential of NANL, its fertilizer efficiency and environmental impact should be considered.

Regarding fertilizer efficiency, the total nutrient content of N and P ($C_{T(N+P)}$) in the NANL was the key parameter. In China, it was reported that the utilization efficiency of N fertilizer and P fertilizer was approximately 25~30 % and 10~25 %, respectively (Ma et al. 2014; Wang et al. 2014b). For example, in the traditional monoammonium phosphate ($NH_4H_2PO_4$) compound fertilizer, the $C_{T(N+P)}$ content was approximately 39 %. If the N loss and P loss were 75 and 90 %, respectively, then the actual nutrient utilization efficiency ($E_{T(N+P)}$) was only approximately 5.7 %. Comparing the actual nutrient utilization efficiency of the NANL under optimal condition ($E_{T(N+P)}$=2.73 %, 2.34 % N+0.39 % P) with that of monoammonium phosphate compound fertilizer, the fertilizer efficiency of the NANL was close to 50 % of it. Further, the N and P adsorbed on the NL was equivalent to the N-P compound fertilizer deposited at a deeper depth. While it was used directly or used in mixture with the conventional fertilizers (N fertilizer, P fertilizer or compound fertilizer) spread over the soil surface, the N contained in the traditional fertilizer could be bonded by the NANL which would also not be easily volatilized (Zhao et al. 2013). On the other hand, NL is a type of clay mineral, and the major components are albite, aluminum oxide, calcite, illite, kaolinite, and quartz, which indicated that the NANL should be nontoxic to the soil environment. Therefore, NANL can be used as either a compound fertilizer or a conventional fertilizer superaddition in agriculture.

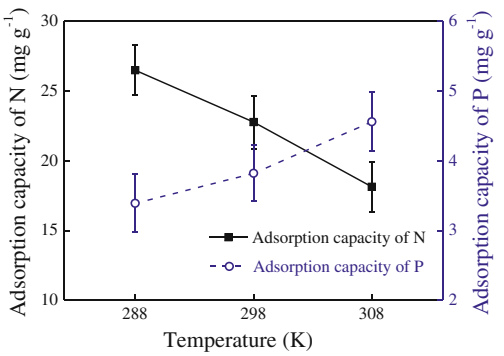

Fig. 5 Effect of temperature on ammonium and phosphate adsorption from urine onto NL

Table 5 Comparison of maximum ammonium and/or phosphate adsorption capability of NL with other reported adsorbents from HU

Adsorbents	Adsorption capacity (mg g^{-1})		References
	Ammonium	Phosphate	
Activated carbon	9.84	0.48	Tettenborn et al. (2007)
Natural zeolite	3.28	0.36	Tettenborn et al. (2007)
HAIX-Fe resin	—	6.9	O'Neal and Boyer (2013)
Clinoptilolite	33.6	—	Beler Baykal et al. (2009)
NL	23.24	4.01	This study

Conclusions

NL was a cost-effective adsorbent for the simultaneous A/R of ammonium and phosphate from HU. The A/R of ammonium was based on ion exchange and molecular adsorption. The calcium phosphate precipitation reaction and the inner-sphere ligand exchange operated in the phosphate A/R. The ammonium and phosphate adsorption capacity was primarily dependent on pH and temperature, and the A/R amount was maximum at an initial pH of approximately 9~10, indicating that HU could be used in practice without any pH adjustment. Ammonium and phosphate A/R onto NL were well described by the pseudo-second-order and Freundlich isotherm models. In addition, both the processes of ammonium and phosphate A/R onto NL were spontaneous; ammonium adsorption was exothermic, while adsorption of phosphate was endothermic. The evaluation of fertilizer efficiency and the determination of environmental friendliness of NANL demonstrated its potential as an available compound fertilizer or conventional fertilizer superaddition for plants.

Acknowledgments This work was supported by the Natural Science Foundation of China (No. 50838005) and the Program for Innovative Research Team in Shanxi Province (Grant No. 2013KCT-13)

References

Akpan-Idiok AU, Udo IA, Braide EI (2012) The use of human urine as an organic fertilizer in the production of okra (Abelmoschus esculentus) in South Eastern Nigeria. Resour Conserv Recy 62: 14–20. doi:10.1016/j.resconrec.2012.02.003

Alshameri A, Yan C, Al-Ani Y, Dawood AS, Ibrahim A, Zhou C, Wang H (2014) An investigation into the adsorption removal of ammonium by salt activated Chinese (Hulaodu) natural zeolite: kinetics, isotherms, and thermodynamics. J Taiwan Inst Chem E 45:554–564. doi:10.1016/j.jtice.2013.05.008

Antonini S, Nguyen PT, Arnold U, Eichert T, Clemens J (2012) Solar thermal evaporation of human urine for nitrogen and phosphorus recovery in Vietnam. Sci Total Environ 414:592–599. doi:10.1016/j.scitotenv.2011.11.055

Barca C, Gérente C, Meyer D, Chazarenc F, Andrès Y (2012) Phosphate removal from synthetic and real wastewater using steel slags produced in Europe. Water Res 46:2376–2384. doi:10.1016/j.watres.2012.02.012

Beler Baykal B, Kocaturk NP, Allar AD, Sari B (2009) The effect of initial loading on the removal of ammonium and potassium from source-separated human urine via clinoptilolite. Water Sci Technol 60:2515–2520. doi:10.2166/wst.2009.614

Boopathy R, Karthikeyan S, Mandal A, Sekaran G (2013) Adsorption of ammonium ion by coconut shell-activated carbon from aqueous solution: kinetic, isotherm, and thermodynamic studies. Environ Sci Pollut Res 20:533–542. doi:10.1007/s11356-012-0911-3

Dbira S, Bensalah N, Bedoui A, Cañizares P, Rodrigo MA (2014) Treatment of synthetic urine by electrochemical oxidation using conductive-diamond anodes. Environ Sci Pollut Res 22:1–9. doi:10.1007/s11356-014-3831-6

Deng L, Shi Z (2015) Synthesis and characterization of a novel Mg–Al hydrotalcite-loaded kaolin clay and its adsorption properties for phosphate in aqueous solution. J Alloy Compd 637:188–196. doi:10.1016/j.jallcom.2015.03.022

Ganrot Z, Dave G, Nilsson E (2007) Recovery of N and P from human urine by freezing, struvite precipitation and adsorption to zeolite and active carbon. Bioresour Technol 98:3112–3121. doi:10.1016/j.biortech.2006.10.038

Guaya D, Valderrama C, Farran A, Armijos C, Cortina JL (2015) Simultaneous phosphate and ammonium removal from aqueous solution by a hydrated aluminum oxide modified natural zeolite. Chem Eng J 271:204–213. doi:10.1016/j.cej.2015.03.003

Hanawa T, Ota M (1991) Calcium phosphate naturally formed on titanium in electrolyte solution. Biomaterials 12:767–774. doi:10.1016/0142-9612(91)90028-9

He Y-F, Zhang L, Wang R-M, Li H-R, Wang Y (2012) Loess clay based copolymer for removing Pb(II) ions. J Hazard Mater 227–228:334–340. doi:10.1016/j.jhazmat.2012.05.071

Huang X (2004) Intersection of isotherms for phosphate adsorption on hematite. J Colloid Interf Sci 271:296–307. doi:10.1016/j.jcis.2003.12.007

Huang H, Xiao X, Yan B, Yang L (2010) Ammonium removal from aqueous solutions by using natural Chinese (Chende) zeolite as adsorbent. J Hazard Mater 175:247–252. doi:10.1016/j.jhazmat.2009.09.156

Huang W-Y, Li D, Liu Z-Q, Tao Q, Zhu Y, Yang J, Zhang Y-M (2014) Kinetics, isotherm, thermodynamic, and adsorption mechanism studies of $La(OH)_3$-modified exfoliated vermiculites as highly efficient phosphate adsorbents. Chem Eng J 236:191–201. doi:10.1016/j.cej.2013.09.077

Hug A, Udert KM (2013) Struvite precipitation from urine with electrochemical magnesium dosage. Water Res 47:289–299. doi:10.1016/j.watres.2012.09.036

Kamiyango MW, Masamba WRL, Sajidu SMI, Fabiano E (2009) Phosphate removal from aqueous solutions using kaolinite obtained from Linthipe. Malawi Phys Chem Earth 34:850–856. doi:10.1016/j.pce.2009.07.012

Kuntke P, Sleutels THJA, Saakes M, Buisman CJN (2014) Hydrogen production and ammonium recovery from urine by a Microbial

Electrolysis. Cell Int J Hydrogen Energ 39:4771–4778. doi:10.1016/j.ijhydene.2013.10.089

Lin L et al (2013) Adsorption mechanisms of high-levels of ammonium onto natural and NaCl-modified zeolites. Sep Purif Technol 103:15–20. doi:10.1016/j.seppur.2012.10.005

Lin L, Wan C, Lee D-J, Lei Z, Liu X (2014) Ammonium assists orthophosphate removal from high-strength wastewaters by natural zeolite. Sep Purif Technol 133:351–356. doi:10.1016/j.seppur.2014.07.010

Lind B-B, Ban Z, Bydén S (2001) Volume reduction and concentration of nutrients in human urine. Ecol Eng 16:561–566. doi:10.1016/S0925-8574(00)00107-5

Liu J, Su Y, Li Q, Yue Q, Gao B (2013) Preparation of wheat straw based superabsorbent resins and their applications as adsorbents for ammonium and phosphate removal. Bioresour Technol 143:32–39. doi:10.1016/j.biortech.2013.05.100

Lǔ J, Liu H, Liu R, Zhao X, Sun L, Qu J (2013) Adsorptive removal of phosphate by a nanostructured Fe–Al–Mn trimetal oxide adsorbent. Powder Technol 233:146–154. doi:10.1016/j.powtec.2012.08.024

Ma L, Feng S, Reidsma P, Qu F, Heerink N (2014) Identifying entry points to improve fertilizer use efficiency in Taihu Basin. Chin Land Use Policy 37:52–59. doi:10.1016/j.landusepol.2013.01.008

Maurer M, Pronk W, Larsen TA (2006) Treatment processes for source-separated urine. Water Res 40:3151–3166. doi:10.1016/j.watres.2006.07.012

MEPC (Ministry of Environmental Protection of China), WWMA(Water, Wastewater Monitoring, Analysis Association) (2002) Comprehensive index and inorganic pollutants. Standard methods for examination of water and wastewater 4th edition. Chinese Environmental Sciences Press, Beijing

National Institute of Standards and Technology (NIST) X-ray Photoelectron Spectroscopy Database (2012) National Institute of Standards and Technology. http://srdata.nist.gov/xps/Default.aspx. Accessed 2012

O'Neal JA, Boyer TH (2013) Phosphate recovery using hybrid anion exchange: applications to source-separated urine and combined wastewater streams. Water Res 47:5003–5017. doi:10.1016/j.watres.2013.05.037

Ohtsu N, Nakamura Y, Semboshi S (2012) Thin hydroxyapatite coating on titanium fabricated by chemical coating process using calcium phosphate slurry. Surf Coat Tech 206:2616–2621. doi:10.1016/j.surfcoat.2011.11.022

Park JH, Jung DI (2011) Removal of total phosphorus (TP) from municipal wastewater using loess. Desalination 269:104–110. doi:10.1016/j.desal.2010.10.048

Perassi I, Borgnino L (2014) Adsorption and surface precipitation of phosphate onto $CaCO_3$–montmorillonite: effect of pH, ionic strength and competition with humic acid. Geoderma 232–234:600–608. doi:10.1016/j.geoderma.2014.06.017

Sangare D, Sou/Dakoure M, Hijikata N, Lahmar R, Yacouba H, Coulibaly L, Funamizu N (2014) Toilet compost and human urine used in agriculture: fertilizer value assessment and effect on cultivated soil properties. Environ Technol 36:1291–1298. doi:10.1080/09593330.2014.984774

Su Y, Cui H, Li Q, Gao S, Shang JK (2013) Strong adsorption of phosphate by amorphous zirconium oxide nanoparticles. Water Res 47:5018–5026. doi:10.1016/j.watres.2013.05.044

Tang X, Li Z, Chen Y (2009) Adsorption behavior of Zn(II) on calcinated Chinese loess. J Hazard Mater 161:824–834. doi:10.1016/j.jhazmat.2008.04.059

Tettenborn F, Behrendt J, Otterpohl R (2007) Resource recovery and removal of pharmaceutical residues treatment of separate collected urine. Institute of Wastewater Management and Water Protection. Hamburg University of Technology, Hamburg

Triger A, Pic JS, Cabassud C (2012) Determination of struvite crystallization mechanisms in urine using turbidity measurement. Water Res 46:6084–6094. doi:10.1016/j.watres.2012.08.030

Udert KM, Wachter M (2012) Complete nutrient recovery from source-separated urine by nitrification and distillation. Water Res 46:453–464. doi:10.1016/j.watres.2011.11.020

Uğurlu M, Karaoğlu MH (2011) Adsorption of ammonium from an aqueous solution by fly ash and sepiolite: isotherm, kinetic and thermodynamic analysis. Micropor Mesopor Mat 139:173–178. doi:10.1016/j.micromeso.2010.10.039

Vanotti MB, Szogi AA, Hunt PG (2003) Extraction of Soluble Phosphorus from Swine Wastewater. Trans ASAE 46:1665–1674

Wang Z, Nie E, Li J, Yang M, Zhao Y, Luo X, Zheng Z (2012) Equilibrium and kinetics of adsorption of phosphate onto iron-doped activated carbon. Environ Sci Pollut Res 19:2908–2917. doi:10.1007/s11356-012-0799-y

Wang X et al (2014a) Highly efficient adsorption of ammonium onto palygorskite nanocomposite and evaluation of its recovery as a multifunctional slow-release fertilizer. Chem Eng J 252:404–414. doi:10.1016/j.cej.2014.04.097

Wang Y, Zhao X, Wang L, Wang Y, Li W, Wang S, Xing G (2014b) The regime and P availability of omitting P fertilizer application for rice in rice/wheat rotation in the Taihu Lake Region of southern China. J Soil Sediment 1–10 doi:10.1007/s11368-014-1047-5

Xie F, Wu F, Liu G, Mu Y, Feng C, Wang H, Giesy JP (2013) Removal of phosphate from eutrophic lakes through adsorption by in situ formation of magnesium hydroxide from diatomite. Environ Sci Technol 48:582–590. doi:10.1021/es4037379

Yang S, Ding D, Zhao Y, Huang W, Zhang Z, Lei Z, Yang Y (2013a) Investigation of phosphate adsorption from aqueous solution using Kanuma mud: behaviors and mechanisms. J Environ Chem Eng 1:355–362. doi:10.1016/j.jece.2013.05.016

Yang S et al (2013b) An electrochemically modified novel tablet porous material developed as adsorbent for phosphate removal from aqueous solution. Chem Eng J 220:367–374. doi:10.1016/j.cej.2013.01.067

Yang L, Wei J, Liu Z, Wang J, Wang D (2015) Material prepared from drinking waterworks sludge as adsorbent for ammonium removal from wastewater. Appl Surf Sci 330:228–236. doi:10.1016/j.apsusc.2015.01.017

Yin H, Kong M (2014) Simultaneous removal of ammonium and phosphate from eutrophic waters using natural calcium-rich attapulgite-based versatile adsorbent. Desalination 351:128–137. doi:10.1016/j.desal.2014.07.029

Zhao Y, Yang Y, Yang S, Wang Q, Feng C, Zhang Z (2013) Adsorption of high ammonium nitrogen from wastewater using a novel ceramic adsorbent and the evaluation of the ammonium-adsorbed-ceramic as fertilizer. J Colloid Interf Sci 393:264–270. doi:10.1016/j.jcis.2012.10.028